Water Masses in the Pacific in CCSM3

LuAnne Thompson
School of Oceanography
University of Washington, Seattle, Washington

Wei Cheng
Joint Institute for the Study of the Atmosphere and the Ocean
University of Washington, Seattle Washington

Corresponding author address: LuAnne Thompson, School of Oceanography, Box 355351, University of Washington, Seattle, WA 98195
E-mail: luanne@u.washington.edu

ABSTRACT

An examination of model water masses in the North Pacific Ocean is performed in the CCSM3 (Community Climate System Version 3) and its ocean-only counterpart. While the surface properties of the ocean are well represented in both simulations, biases in thermocline and intermediate water masses exist that point to errors in both ocean model physics and the atmospheric component of the coupled model. The lack of NPIW (North Pacific Intermediate Water) in both simulations as well as the overexpression of a too fresh AAIW (Antarctic Intermediate Water) are indicative of ocean model deficiencies. These properties reflect the difficulty of low-resolution ocean models to represent processes that control deep water formation both in the Southern Ocean and in the Okhotsk Sea. In addition, as is typical of low resolution ocean models, errors in the position of the Kuroshio (the North Pacific subtropical gyre WBC, western boundary current) impacts the formation of the water masses that form the bulk of the thermocline as well as the properties of the NPIW. Biases that arise only in the coupled simulation include too salty surface water in the subtropical North Pacific and too deep a thermocline, the source of which is the too strong westerlies at mid-latitudes. Biases in the location of Intertropical Convergence Zone (ITCZ) and the South Pacific Convergence Zone (SPCZ) lead to the opposite hemispheric asymmetry in water mass structure when compared to observations. The atmospheric component of the coupled model acts to compound most ocean model biases.

1. Introduction

The climate modeling community is working to improve model physics in all components of the coupled system. Many of the remaining issues involve subgrid scale processes not resolved by model grids, including processes that occur on shelves under sea-ice, tidal mixing in small passages, and the consequences of too low Reynold's number required by low resolution. Currently, ocean models in climate scale simulations are typically run at one-degree resolution with increased resolution in the tropics. The model solutions at mid-latitudes continue to be limited by resolution (for instance, see Weese and Bryan, 2006) where the models do not resolve the internal radius of deformation, and thus do not resolved eddies that arise from baroclinic instability. Low resolution also leads to a poor representation of the mean flow field, with a primary example being the well known bias in the latitude of western boundary current separation. In addition, some processes are simply missing from most models, such as tidal mixing or interaction of dense water plumes with topography, which is known to be important in the formation of certain water masses in the world's ocean. Initial condition and boundary condition (including surface forcing) errors can also result in errors in ocean model simulations.

Because the surface ocean directly interacts with the atmosphere, previous studies have focused on identifying biases in surface properties. For example, Large and Danabosoglu (2006) found that the surface ocean temperature and salinity in the CCSM3 are reasonably well represented except for in isolated regions where known errors in ocean physics are expected to occur, such as in regions with deep water formation, under

sea ice, and in the highly non-linear western boundary currents. The relatively small differences in sea surface salinity between the coupled model results and the observations that occur over the large scale predominantly reflect errors in the precipitation field. Large and Danabosoglu (2006) show that the surface salinity is too high in the CCSM3 in the Pacific subtropical gyre and in the eastern tropical Pacific. South of the equator, the surface salinity is too low, reflecting the tendency for the coupled model to produce a too strong SPCZ (South Pacific Convergence Zone). In both cases, the surface salinity anomaly is attributed to errors in the precipitation field owing to biases in the larger scale structure of the tropical atmosphere. An overshoot of the separation point of the Kuroshio is also noted.

Even small errors in surface properties can propagate into the interior of the ocean where they can accumulate and persist especially where the ocean memory is long such as in deep and intermediate waters. In addition, errors tend to be enhanced by coupling. Gent et al (2006) examined CFC (Chrlorofluorocarbon) and heat uptake in CCSM3, the model results were once again in qualitative agreement with observations, with local problematic spots. One of those spots is in the western Pacific and Indian Ocean near Antarctica and along the path of the Antarctic Circumpolar Current. Both an ocean-only and a coupled simulation tend to show production of too much deep water off of Antarctica in the Pacific and Indian Ocean sectors. The penetration depths of CFCs are otherwise well represented in the Pacific, with some small quantitative deviations from the observations. For instance, the deepest CFCs in the subtropical North Pacific show too deep of penetration in the western North Pacific Kuroshio Extension region with maximum penetration depth in the subtropical gyre further to the east than in the

observations and less confined spatially. This feature is again related to the overshoot of the western boundary current. In the Southern Ocean, however, the coupled simulation shows improvement in representation of CFCs over an ocean-only run between 40° S and 60° S owing to stronger winds in the coupled-model that compensate for errors in the ocean model physics (Gent et al, 2006 and see discussion below).

Because water mass distributions have important implications for ocean heat and chemical tracer storage, in this paper, we examine modeled thermocline and intermediate water mass structure in the Pacific Ocean, and identify the possible sources of model biases. We chose this ocean because deep water is not formed in the North Pacific. The upper ocean dynamics are governed primarily by wind driven effects and fit into existing theories. In addition, flow throughout the thermocline and into the intermediate water will be spun up in a century, whereas in the Atlantic, the circulation would still be undergoing significant adjustment on these time scales. Finally, the extratropical Pacific connects directly to the Tropical Pacific, an important region for setting the state of the global climate.

As in any model evaluation, the metric by which a model is measured determines whether the model is considered a success. The two areas of the water column that we focus on here are the thermocline waters in the subtropical gyre and the intermediate waters that originate in the subarctic gyre in the North Pacific and in the Southern Ocean. We first examine the subsurface properties of the coupled model and compare them against an ocean-only simulation, and against an ocean climatology. Next, we examine atmospheric forcing, both buoyancy flux and wind stress, and determine their relationship to the subsurface properties. Because the thermocline waters are formed primarily in

regions where there are local maxima in MLD (mixed-layer depth), we pay particular attention to the causes of localized regions of maximum MLD. We end with a discussion of the potential consequences of the biases in the North Pacific for the CCSM3 modeled climate.

2. Models and Data

CCSM3 is a well-documented state-of-art coupled climate model, and more information can be found at http://www.ccsm.ucar.edu (see the June 2006 issue of Journal of Climate for a complete analysis of the model construction and performance). Here we only give a brief introduction of the runs we analyzed. The atmospheric component in the coupled model uses a T85 spectral truncation (equivalent to 1.4^o X 1.4^o grid spacing) and 26 vertical levels. The radiative forcing is fixed at 1990 levels for anthropogenic greenhouse gases, ozone, and aerosols. The ocean and sea-ice models share the same horizontal grid, with approximately one-degree longitudinal resolution and variable latitudinal resolution that is finer near the equator (approximately 0.3°). The ocean component is described in detail in Gent and Danabasoblu (2004). The Gent and McWilliams (1990) parameterization is used which mixes along isopycnals with a Laplacian operator with diffusion value of 600 m^2s^{-1} and uses an additional eddy induced transport of tracers. The SSS is relaxed back to observations with a time scale of four years. There are 40 levels vertically in the ocean model. The data used in this study is from years 300-599 of the 1000 year control simulations. All data were saved as monthly averages during the run. We term this run CPL.

To understand to what extent biases in the water mass structure in the coupled

model stem from internal ocean model physics versus from surface forcing, we also examined simulations by the stand-alone ocean component of CCSM3, the Parallel Ocean Program model, driven by prescribed atmospheric forcing The forcing is based on the Common Ocean-ice Reference Experiments (CORE, available at http://data1.gfdl.noaa.gov/nomads/forms/mom4/CORE.html), constructed as a repeated annual cycle. The atmospheric forcing is applied via bulk aerodynamic formulae for the turbulent fluxes using model SST (sea surface temperature), and virtual salt flux is used for forcing the sea surface salinity. No extra surface restoring is used for SST, while SSS has a restoring flux with time scale of 91 days. The model is run for 120 years, and we used the last 10 years data in this analysis. We term this run OCN. Where applicable, model simulated upper ocean temperature and salinity as well as MLD are compared against observational data in WOA01 (World Ocean Atlas 2001, Cronkright, 2001). The MLD in WOA01 is defined based on a variable potential density criterion corresponding to density change of 0.125 kg m^{-3}. We use the same criterion to define the modeled MLD for consistency.

3. Model Water Mass Structure

Salinity in the Pacific Ocean provides a useful tracer for different water masses because of the strong halocline in the subarctic gyre, and the fresh signature of both intermediate waters in the basin. In the central Pacific in WOA (Fig. 1a), the low salinity water that emanates from high latitudes at 400 to 600 m tracks the AAIW (NPIW) in the southern (northern) hemisphere respectively. The southern hemisphere subtropical thermocline water (from the surface to roughly 400m) is saltier than its counterpart in the northern hemisphere, and has a more direct connection to the tropical thermocline.

The characteristics of the observed water masses can also be seen in both CPL and OCN. In both models, the AAIW (designated by the large low salinity tongue reaching from the Southern Ocean into the subtropics) dominates the section at intermediate depths from the base of the thermocline to almost 1000 m depth (Fig. 1). At the same time, NPIW (designated by the 34.2 salinity contour) is absent outside of the subarctic gyre (Fig. 1b). This bias is less pronounced but still present in OCN (Fig. 1c), where the low salinity tongue of AAIW can be seen reaching almost to the equator, while the NPIW does not appear south of 40° N as it does in the observations. In CPL, the subtropical waters in the Northern Hemisphere, which are significantly saltier than in the observations are the dominant source of water for the tropical thermocline. OCN does a much better job of capturing the observed north-south structure of the salinity in the thermocline, although it is still slightly too fresh in the Southern Hemisphere, and too salty in the Northern Hemisphere. It is important to keep in mind that there is restoration to observed surface salinity in OCN that forces modeled surface salinity to be close to observations.

The pathways of water masses described above can be examined by considering salinity distributions on density surfaces (Fig. 2). Based on structure of the salinity in the vertical (Fig. 1), we pick the σ_θ =26.8 (25.6) kg m^{-3} (potential density) surfaces to represent the intermediate (thermocline) waters. On the 26.8 kg m^{-3} σ_θ surface, the subarctic gyre is significantly fresher than the subtropical gyre in the observations (Fig. 2b). The fresh tongue of the NPIW extends to nearly the equator. However, in CPL the NPIW is confined to the subarctic North Pacific, and separated from the AAIW by a salty pool of water (Fig. 2d). OCN also has NPIW confined to the subarctic North Pacific,

although there is a remnant of fresh water that emanates from the Northeast Pacific (Fig. 2f). At the same time, water from the Southern Hemisphere is too fresh (Fig. 2f)

On the shallower σ_θ surface (25.6 kg m^{-3}), (Fig. 2 a, c, and e), the relatively fresh water in the subarctic gyres in both hemispheres is seen. In observations, the Northern Hemisphere water meets the saltier southern hemisphere water just north of the equator in a well defined salinity front (Fig. 2a). OCN captures that front in essence, however, there are two tongues of fresh water that underlay the subtropical and tropical thermocline instead of the one broader tongue in the observations. In contrast, in CPL while there is a fresh signal that works its way along the eastern boundary and into the tropics as in the observations (Fig. 2c), the entire subtropical region is significantly saltier than in either observations or in OCN. As we show below, this occurs because the subtropical gyre extends too deeply when compared to the observations, and the source of this error can be traced back at least partly to atmospheric forcing.

On both isopycnals, OCN shows distinct tongues of fresh water that penetrate into the subtropics from the eastern boundary; this is repeated in CPL on 25.6. The observations present a smoother picture, with less of a distinctive advective signals. This suggests that both models lack along-isopycnal mixing necessary for mixing water masses on these isopycnals. This is consistent with the results of Mecking et al (2004) who found that in a diagnostic model of CFCs in the subtropical North Pacific where currents are derived from the observed density distribution, isopycnal mixing, owing to mesoscale eddies, has to be included to accurately represent the spreading of CFCs into the interior of the subtropical gyre. They found that an along isopycnal diffusion coefficient with value of 2000 m^2 s^{-1} was needed in the interior and an even larger value

of 5000 $m^2 s^{-1}$was need in the Kuroshio Extenion. This contrasts with the much smaller value of 600 $m^2 s^{-1}$used in ocean component of CCSM. However, a simple increase in this value would not improve model performance as that would act to degrade the representation of the mean flow field as well.

4. Factors determining Model Water Mass Structure

Water mass structure in the world's ocean is ultimately determined by both internal ocean physics and by surface forcing. In this section, we discuss these factors and their influences on MLD, which in turn regulates vertical water mass structure.

a. The physics of water mass formation in previous studies

Below the thermocline and above the deep water masses lay intermediate waters. NPIW is thought to originate at least partly in the Okhotsk Sea where dense water is formed on the shallow shelf, and then tidal mixing through narrow passages modifies the water that then mixes again in the mixed-water region of the Kuroshio-Oyashio Current system (Talley, 1993, 1997, Yasuda et al, 1996). Clearly, these mixing processes are beyond the ability of any low resolution or even high resolution global ocean model; previous attempts including tidal mixing in an ad hoc basis led to improvements of the representation of NPIW (Yamanaka et al, 1998). Nakamura et al. (2006) were able to successfully reproduce NPIW using and OGCM that takes into account the tidal mixing in the passages between the Kuril Islands that separate the Okhotsk Sea from the open North Pacific. While some experimentation has been done on the inclusion of tidal mixing in coupled climate models (see for instance Montenegro et al, 2007), the resolution of the models is not adequate to represent the effects of tidal mixing in the passages described above. The detailed structure of the subarctic water masses is

complex with a subsurface temperature minimum, and a intermediate temperature maximum (Ueno and Yasuda, 2000) which global scale ocean models also do not reproduce. Kobayashi (1999,2000) show that if the Kuroshio is located too far north in a model, too light and fresh NPIW is formed (which they term false NPIW), forming near the separation of the Kuroshio from the coast and staying near the surface.

It has long been known that AAIW is also difficult to simulate correctly with too fresh AABW (Antarctic Bottom Water) occurring in models owing to too low of salinity on the shelf (England, 1992). Thus, AAIW depends not only on interior ocean mixing processes, but also indirectly through the AABW, on processes that occur in a small region, in this case, the Weddell Sea and Ross Sea Shelves. Doney and Hecht (2002) in a lower resolution simulation than the one discussed here show that the deep-water ventilation in the Ross and Weddell Seas is too weak in their model. As the deep water masses traverse away from the source regions, they warm and freshen faster than in the observations, particularly near the source regions. In addition, the influence of sea-ice on the surface properties in the source region were of concern.

In the thermocline, there are three distinct mode waters in the North Pacific with two having counter parts in the South Pacific: the CMW (Central Mode Water) that forms in the Central North Pacific north of the Kuroshio Extension front with temperatures of 9-13°C; the subtropical mode water (STMW) that forms in the Western North Pacific south of the front and south and west of the CMW with temperatures of 15 to 18°C (Suga et al 2004); finally, the ESMW (Eastern Subtropical Mode water, Hautala and Reommich, 1998) forms in the Eastern North Pacific and has similar temperatures as STMW but forms further east of the STMW and is geographically distinct. For these

mode waters preconditioning plays a large role, evidently by their co-location with localized maximum MLD (mixed-layer depth). STMW and CMW are not distinct in low resolutions models because of the biases in the representation of the Kuroshio Extension, both of which are formed south of the front in models (Ladd and Thompson, 2001). ESTMW differs from the other two in that it forms in a "stability gap" (Hautala and Roemmich, 1998) that results from the proximity of the temperature stratified subtropical gyre and the salt stratified subarctic gyre (Ladd and Thompson, 2000) and its proper representation relies on the maintenance of that stability gap. The subarctic region is particularly sensitive to atmospheric forcing owing to the presence of the salinity controlled thermocline which results from precipitation exceeding evaporation (Emile-Geay et al, 2003).

b. Wind stress forcing and the Sverdrup relation

In the North Pacific, the circulation is primarily driven by the wind through Sverdrup dynamics as there is little overturning circulation associated with deep water formation. The too strong surface westerlies in CPL in mid-latitudes have been noted by previous authors (Collins et al a, 2006, their Fig. 1, and Collins et al 2006 b, their Fig. 11). Gent et al (2006) point to the excess westerlies in the southern hemisphere that lead to a better representation of CFC penetration in the South Atlantic in the CPL simulation over the OCN simulation. It appears that the penetration depth is improved as well in the subtropical North Pacific; with the too large surface westerlies compensating for the lack of along-isopycnal mixing in the models.

The Sverdrup relation predicts that the meridional transport integrated from the surface to the base of the thermocline is directly proportional to the curl in the wind-stress

$$\beta \int_{z=-H}^{0} v dz = f W_E \qquad (1)$$

Where, β is the meridional gradient of the Coriolis parameter *f*, *v* is the meridional velocity outside of the boundary current, W_E is the Ekman Pumping, given by $W_E = \hat{k} \bullet \nabla \times \tau / f\rho$, z is the vertical coordinate with $\hat{k}$ the vertical unit vector, τ is the wind-stress, and ρ is the density of sea water (given by 1025 kg m^{-3}), and H is the depth of the wind driven layer. By integrating (1) zonally from east to west, an estimate of the wind-driven component of the circulation can be made. The vertically integrated circulation carries about 50 Sverdrups in the subtropical gyre in CPL (Fig. 3). Using the wind-stress from CPL, the Sverdrup transport derived from (1) shows good agreement with the barotropic transport streamfunction taken directly from CPL outside of the western boundary current region in the subtropics (Fig. 3 a and c); the same agreement also exists in OCN between its wind derived Sverdrup transport and barotropic stream function (Fig. 3d). However, when comparing the wind-derived Sverdrup transport in OCN and CPL (Fig. 3 a and b), it is apparent that the too large zonal wind-stress leads to a significant enhancement of the transport in the subtropical gyre in the coupled simulation.

A consequence of the error in the strength of the mid-latitude wind-stress is that the thermocline is too deep. The theory developed by Rhines and Young (1982) leads to an advective scaling for the thermocline depth D_a (Vallis, 2006, eq. 14.130)

$$D_a = \left(\frac{f^2 W_E L}{\beta \Delta b} \right)^{1/2} \quad (2)$$

where L is the width of the gyre, Δb is the buoyancy difference across the subtropical gyre in the latitudinal direction, or equivalently the buoyancy difference across the thermocline. This estimate assumes that the diapycnal diffusion is small in the thermocline. In the ocean model, the diapycnal diffusion in the upper ocean is determined by the Large et al (1994) KPP (K-profile parameterizaion) scheme and is about $1X10^{-5}$ m ^{2} s $^{-1}$ and it likely sufficiently inviscid for the scaling to hold. The strength of the wind is about 25% larger in CPL than in CORE, and according to the scaling in (2), the thermocline depth would be about 10% deeper on average. To determine the depth of the thermocline, we found the location in the vertical where the stratification is maximum outside of the mixed-layer. Averaging the thermocline depth from WOA01 between 130°E to 170°E and 25°N to 35°N, we find an average thermocline depth of 300 m, while in CPL (because of the overshoot of the western boundary current we averaged over a slightly different region) between 24°N to 40°N and 145°E to 180°E we find an average thermocline depth of 340m, in agreement with the scaling argument.

There are deviations between the predicted Sverdrup transport from theory and the barotropic transport at the both the western and eastern ends of the section (Fig. 3d). Near the western boundary, the vorticity balance that leads to (1) does not hold because viscous and non-linear processes begin to play an important role. In the eastern basin, near 160°W, there is a significant deviation from the Sverdrup balance in both CPL and OCN. It is interesting to note that Hautala et al (1994) saw the same deviation in observations, that is, the meridional transport calculated from a density section showed a

deviation from (1) at the same location and with similar longitudinal structure. This deviation is associated with the formation region of the ESTMW and most likely is owing to a significant contribution to meridional transport from the thermohaline circulation associated with this mode water production.

In addition, the strength of the wind driven circulation is directly reflected in the zonally averaged MOC (meridional overturning circulation) in the Pacific ocean where the thermohaline circulation is small (Fig. 4). Consistent with the results shown by ocean tracer fields (salinity in our case), the MOC shows a different asymmetry about the equator between CPL and OCN. The maximum value for the MOC north of the equator is smaller than south of the equator in OCN, but the opposite relationship holds in CPL. In addition, the MOC is shallower in OCN by several hundred meters north of the equator than in CPL. This results in more water feeding the equatorial thermocline from the Northern Hemisphere in CPL, which enhances the surface driven errors in the subsurface salinity distribution at the equator.

c. Surface buoyancy forcing

One difficulty with determining the relative importance of surface forcing versus ocean circulation on water mass structure is that surface forcing from observations is only known within large error bars. While errors in modeled SST (sea surface temperature) and SSS (sea surface salinity) exist, since sea surface salinity (SSS) cannot feed back directly onto the atmosphere, getting SSS correct is a particularly stringent test for a coupled model. In most cases, ocean-only models, such as OCN, are run using some level of SSS relaxation. This, combined with the natural relaxation of SST through the calculation of turbulent heat fluxes by bulk formulae, results in reasonably well

represented SST and SSS in OCN (Fig. 5c and d), although quantitative differences still exist. Annual mean SSS biases in OCN are within 0.5 psu throughout most of the Pacific ocean. The exceptions are the central subtropical gyre which is too salty by over 0.5 psu and the western boundary current region that is too salty south of the Kuroshio Extension and too fresh north of it.

A fresh surface intensified water mass forms north of the front which is akin to the false NPIW discussed in Kobayashi (1999). This water mass forms in response to fresh surface water leaving the Okhotsk Sea, while deep water that is a component of NPIW is not formed correctly on the Okhotsk Sea Shelf. In most of the subarctic gyre, the SSS remains too fresh in OCN as this false NPIW permeates the surface ocean. There is a region of too salty surface water in the northwest Pacific that is coincident with too deep mixed-layers which are discussed in the next section. CPL shows a similar SSS bias (Figure 5b), but with larger magnitudes in the subtropics, and smaller magnitudes in the Kuroshio Extension region than in OCN. The smaller magnitude of bias in CPL is likely owing to the compensating effect of the too salty subtropics water that mixes into the modeled subarctic gyre near the western boundary. In addition, there is a fresh bias south of the equator in CPL owing to the double ITCZ in CPL which is discussed further below. SST biases in CPL are much larger than those seen in OCN (Figure 5 a), with the cold tongue bias more pronounced. In OCN, SST is only noticeably different from observations near the separated western boundary current region. The separated western boundary current appears to be the source of most of the errors in CPL with the error having larger spatial scale, with the SST too warm north of the Kuroshio Extension, too

cold within the Kuroshio Extension, and then again too warm south and east of the Kuroshio Extension.

The differences in sea surface properties between CPL and OCN stem from differences in surface forcing as well as possibly differences in advection caused by differences in ocean currents. To examine the role of surface forcing, we compare the surface forcing in CPL and OCN, recognizing that the forcing in OCN is modified by both the model SSS and SST. Compared to OCN forcing, CPL shows excessive precipitation south of the equator as a result of its too strong SPCZ (Fig. 6a, Large and Danabasoglu, 2006), and a deficit of precipitation centered around 30° N and 30° S where surface evaporation is also too strong due in part to the surface wind biases mentioned earlier. The resulting differences in net surface freshwater flux are in general consistent with the SSS differences between the two runs (Fig. 5b and d). However, despite the comparable net freshwater flux differences in the northern and southern mid-latitudes, the SSS difference between the two models (Fig. 5b and d) appears much stronger in the northern hemisphere than in the Southern Hemipshere, suggesting a prominent role of non-local effects. A measure of the combined effects of errors in ocean circulation and surface fresh water forcing is the relaxation component of the fresh water forcing used in OCN. Its magnitude is less than twenty percent of the imposed fresh water flux; however, its spatial pattern reflects the errors in the surface salinity field (Fig. 6b). In the subtropics it acts to reduce excess salinity in the model. The too fresh bias near 40° N is also compensated at least partially by the relaxation.

While it is possible to attribute SSS biases in a coupled model to either surface forcing or ocean advection, thermal damping of SST anomaly by surface heat flux makes

the relationship between SST, surface heat flux, and ocean transport of heat less apparent. OCN latent heat fluxes are similar to those predicted from NCEP (National Center for Environmental Prediction) using observed SST (not shown), and within the known errors of the observationally derived fluxes. To understand the differences in SST in OCN and CPL, it is important to compare the surface fluxes that force the two model oceans to each other. It is important to keep in mind that the turbulence surface fluxes that force OCN are calculated using model SST and thus are different from those calculated using observed SST. The radiative fluxes in OCN however, reflect observations. The turbulent and short wave flux differences tend to compensate each other in the annual mean. But, there are differences in the total heat flux between OCN and CPL (Figure 6c). In the northern hemisphere, the CPL ocean looses more heat to the atmosphere than the OCN ocean, with a net cooling of up to $20 Wm^{-2}$, while in the southern hemisphere mid to high latitudes CPL consistently gains more heat than OCN. Despite these surface flux differences between OCN and CPL, in the NH, the SST in CPL is consistently higher than SST in OCN, indicating that such SST differences are driven by ocean advection. The same is also true in the SH.

The tropical heatflux-SST relationship is more complex and deserves further discussion. On the equator, in a zonally averaged sense, the two models have the same SST, although both are colder than the observations. CPL shows anomalous heating at the equator relative to OCN (Figure 6c), mostly owing to turbulent heat flux differences associated with smaller trade winds in CPL. In addition, the equatorial short wave radiation is smaller in CPL relative to CORE, possibly owing to errors in cloudiness in the atmospheric component of the coupled model, which somewhat compensates the

local turbulent heat flux differences. Directly south of the equator at 5°-10°S, the SST warms more in CPL than in OCN while the total surface heat flux anomaly (CPL-OCN) is out of the ocean. This net cooling effect is dominated by shortwave radiation, which is likely related to the enhanced SPCZ/double ITCZ in CPL.

d. Mixed-layer Depth

An important component of thermocline water masses is mode waters that form in regions of local maximum in MLD (Ladd and Thompson, 2000). MLD gradients via lateral induction is an important factor for creating regions of maximum subduction (see for example Qiu and Huang,1995). There are three regions of local MLD maximum in the model North Pacific, one in the subarctic gyre in the northwest Pacific, the next is in the Kuroshio Extension, and the third is in the Eastern subtropical Pacific (Fig. 7). The last two regions have local maximum in MLD in climatological observations as well. The maximum in MLD occurs in late winter, and is associated with weak stratification and/or large surface heat loss from the ocean. The observed two MLD maximum associated with CMW and STMW formation (Fig. 7a) coalesce in the model into one large region in the western basin around 30°N to 40°N (Fig. 7b, c). This occurs in both CPL and OCN and is related to the bias in the separation point of the WBC. As was seen in Ladd and Thompson (2001), in low-resolution models, both water masses form south of the subtropical front, with the STMW preconditioning the formation of CMW. This results in an over-expression of CMW that becomes a major component of the water masses in the model thermoclines. In the eastern subtropical North Pacific, once again the region of local maximum in MLD is larger, and the maximum MLD deeper, in the models than in the observations.

To determine the dominant causes for the modeled MLD biases, we perform a series of sensitivity experiments using the mixed-layer model from the CPL and OCN in a one-dimensional form using the KPP scheme. We used forcing fields diagnosed (radiative flux and latent and sensible heat flux, wind stress) from the model (OCN or CPL) and/or observations to force the one-dimensional model. Nine experiments were performed for each patch of local MLD maximum using OCN, CPL, and WOA for the initial conditions, and OCN, CPL surface forcing fields, and surface forcing based on the COADS (Comprehensive Ocean Data Set, daSilva et al, 1995), neglecting forcing associated with ice-formation processes such as brine rejection and fresh-water flux owing to ice-melt. For consistency with observational analyses and the monthly sampling intervals from the models, we calculate the MLD using the criterion described earlier. We begin the one-dimensional simulations in September when the water is the most stratified, and run the model for a year using monthly forcing interpolated on to the model time step. In all cases, the representation of re-stratification in the spring is too abrupt relative to the observations. This is typical of one-dimensional models and reflects the limitations of both the monthly forcing and that when the mixed-layer is in the shoaling phase, it immediately detrains such that the MLD is the Monin-Obukhov depth where mechanical mixing by stiring is balanced by the restratification effect of heating.

In the subarctic North Pacific, region A in Figure 7 (Fig. 8 a,d,g,j), we see that using CPL, WOA or CPL initial conditions combined with either OCN or COADS forcing fields gives very similar results. Using CPL forcing however, we find that the one-dimensional model consistently underestimates MLD. It is particularly striking that

the CPL forcing gives maximum MLDs in the one-dimensional model that are only half of the MLD in the full coupled simulation (Fig. 8a). As seen in Fig. 8 of Collins et al (2006a), in CPL annual mean sea-ice exists outside of the Okhostk sea and on the eastern side of the Kamchatka Peninsula, whereas in observations the region is ice-free. The sea-ice formation and subsequent brine rejection deepens the MLD in CPL, however, brine rejection was ignored in the forcing that we applied in the one-dimensional model, leading to an underestimation of the MLD in the one-dimensional model relative to the full model. The deep mixed-layers in this region in CPL may contribute to the too high salinity at the surface since in the subarctic gyre, there is a subsurface salinity maximum in the models that can be accessed by the surface when the MLD is deep.

In the Kuroshio Extension (region B in Fig. 7), the western boundary current in CPL and OCN is located well to the north of where it is in the observations. This results in MLDs that are too deep in the Kuroshio Extension because the Kuroshio in the models bring warm water too far north, and that water is then cooled vigorously by the cool air coming off of Asia in winter. The MLD from the one-dimensional model reproduces both CPL and OCN MLDs (Fig. 8 b,e,h,k) and suggests that the MLD evolution in the full model run (CPL and OCN) in this region is dominated by one-dimensional physics. However, the observed MLD is much shallower than the prediction from all the one-dimensional simulations irrespective of the initial condition or forcing. This suggests that in the real ocean, one-dimensional physics does not apply on the seasonal time scale for mixed-layer depth prediction. In particular, the time scale for advection in the real ocean to restratify the water column is shorter than a year, while in the models advection by the western boundary current takes longer than a year to restratify the water column. In this

analysis the we cannot distinguish between lateral advection by the mean flow and lateral mixing by the parameterized eddies (which is ultimately an advective process).This highlights the impact of too weak currents on MLD evolution and water mass formation.

In the eastern subtropical North Pacific (region C in Fig. 7), CPL and OCN produce far larger MLDs than is seen in the observations, with the initial stratification making a profound difference in the maximum MLD (Fig. 8 c, f, i, l). The initial conditions determine the evolution of the MLD much more than the forcing fields do (notice the similarity of the three lines within each of the plots in Fig. 8f, i and l). This argues that there are errors in the stratification in the region in both CPL and OCN. Ladd and Thompson (2000) showed that the local maximum in MLD in the region depends on the presence of a buoyancy gap (described in Hautala and Roemmich, 1998). The line demarking the zero in the wind stress curl turns to the south along the eastern boundary (the negative barotropic transport seen in Fig. 3a, b and c near the eastern boundary between 20° N and 40° N). The formation region for ESTMW is located at the boundary between the subtopical gyre in a region of weak stratification where the temperature stratifcation of the subtropical gyre meets the salinity stratification of the subarctic gyre. This region of weak stratification is too large in both CPL and OCN and results in a wide spread region of locally deep MLDs.

The weak stratification in the eastern subtropical North Pacific in the models occurs for a different reason than in the observations. Further examination of the observed region of maximum MLD shows MLDs deeper than 100 m in a north-south swath that is offshore of the region of the Ekman suction off the coast of California (Figure 7). In contrast, the region of MLD deeper than 150m in the models occurs

primarily to the south and west of the region of maximum MLD in the observations. The stratification is controlled by temperature there; there is a region of weak stratification below the seasonal thermocline. This water originated in the central Pacific and is a remnant of the CMW. The connection between the three different mode waters in the NP, the STMW, the CMW, and the ESTMW is strong in the models, with STMW preconditioning the CMW. The weak stratification in the subtropical thermocline that is formed in the Kuroshio Extension then makes a widespread ESTMW possible. The pervasive influence of the western boundary current location and properties on the structure of the water masses in the entire subtropical gyre is highlighted by these tightly linked mode waters.

5. Discussion

The major water masses in the Pacific Ocean can be identified using potential temperature-salinity relationships (Fig. 9) and the model biases are clearly identified. At 40° N at the surface the temperatures are reasonable in both OCN and CPL, but the salinity is much too low in OCN with CPL modestly better (Fig. 9a). As in Kobayashi (1999,2000), this reflects the presence of the surface false NPIW. The too fresh and surface intensified NPIW is ameliorated in CPL by the too salty subtropical gyre. In the middle of the thermocline at σ_θ =26.0 kg m^{-3}, both OCN and WOA show a salinity maximum owing to thermocline water that originates in the subtropics; the salinity maximum occurs at a denser level near σ_θ =26.8 kg m^{-3} in CPL, which also originates in the subtropical gyre (see also Fig. 1b), but penetrates deeper owing to the too deep thermocline in CPL. The bias owing to the lack of a strong NPIW in OCN results in a weaker salinity minimum at σ_θ =26.8 kg m^{-3}than in observations, while in CPL there is

no salinity minimum between σ_θ 26 and 27 kg m^{-3}. Instead, in CPL, a salinity minimum appears at a denser isopycnal, and reflects the pervasive influence of AAIW. In the deepest part of the water column, there is good agreement, between observations, OCN and CPL, partially reflecting that the deep water in this region is the oldest water mass in the world, and the water mass structure has probably not completely lost its memory of the initial conditions in either model run.

Moving south into the subtropical gyre (at 20N, Fig. 9b), both models are too salty over nearly the entire water column, with once again OCN showing larger errors at the surface than in CPL, although the region of too high SSS in CPL is much more pervasive than in OCN (Figure 5b,d); we note that the stratification does show that it is salinity dominated in the upper ocean at 40N (Figure 9a) while it is temperature dominated at 20N (Figure 9b). Both models show a too strong subsurface salinity maximum between σ_θ =24 and 25 kg m^{-3} which is associated with the too strong and too salty mode waters (a combination of STMW and CMW), and a too weak (in OCN), or nonexistent (in CPL) subsurface salinity minimum associated with the NPIW. Once again, the salinity minimum in CPL occurs on a denser isopycnal than in the observations that comes from the arrival of too fresh AAIW into this region. At the equator (Fig. 9c), OCN does very well in the upper ocean, while CPL begins to deviate substantially from the observations. The fresh signal just below the surface in CPL reflects errors in the source regions, contributed by the modeled double ITCZ. Below σ_θ =26.0 kg m^{-3} the too fresh AAIW in both model runs maintains a too strong salinity minimum. At 20°S (Fig. 9d), CPL deviates further from the observations as it is too fresh water throughout the entire water column, with OCN showing similar, but weaker biases, with OCN matching

the observations well near the surface. There is a subsurface salinity maximum in the subtropical water near σ_θ =25 kg m^{-3}, with the value of the salinity maximum lower in CPL owing to the too fresh surface source waters. The too fresh salinity minimum near σ_θ 27.0 kg m^{-3} associated with the AAIW in both models can be seen. This feature is more pronounced at 40° S (Fig. 9e) as it is closer to the source region of the too fresh model AAIW.

6. Conclusions

While ocean GCMs and coupled climate models have improved remarkably in recent years, long standing problems still exist in reproducing observed ocean circulation and water mass properties. In addition, biases in the atmospheric components of coupled models often reinforce biases in the model ocean. For the Pacific Ocean, biases that result from the mis-represetation of ocean physics come primarily from three regions. First, the misrepresentation of small scale physics associated with intermediate and deep water formation lead to water mass biases in the Northwest Pacific as well as in the Southern Ocean. The errors are more profound in the Northern Hemisphere where the lack of NPIW contributes to a too salty subarctic gyre and a too salty and deep subtropical thermocline. The second problematic region is in the western boundary currents in northern hemisphere subtropical gyre, where the WBC in non-eddy resolving models separates from the coast too far poleward by as much as 5^o of latitude. This leads to water mass biases throughout the subtropical North Pacific. There is an overexpression of CMW or equivalently an over expression of a too cold version of STMW. This misrepresentation of the thermocline water masses also contributes to the exclusion of NPIW from the subtropics, and potentially to the overexpression of

ESTMW, which is the third problematic region. One consequence of the misrepresentation of the extratropical water masses is that there is an overexpression of North Pacific water as a source water for the tropical thermocline. In the southern hemisphere, the fresh bias in AAIW that has been found in other modeling studies also appears.

On the other hand, some biases in the coupled simulation can be traced to and/or enhanced by errors in components other than the ocean of the coupled system. Main problems of this kind are identified as follows: the first is the presence of ice in the NW subarctic gyre where deep mixed-layers form in CPL owing to brine rejection. We infer this from the one-dimensional KPP simulations using forcing fields from CPL, but without the inclusion of brine rejection. The second more profound problem with the model simulations related to atmospheric circulation is the too strong surface winds in the subtropics where the thermocline responds by being far too deep. This couples with the overshoot in the western boundary current and subsequent formation of an unrealistically large mode water mass gives a much larger than observed subsurface salinity maximum. These errors reach into the tropics through the meridional overturning circulation which is also strengthened by the strong winds in the subtropics and results in too much North Pacific water relative to South Pacific water in tropical thermocline ventilation. Lastly, biases in the tropical atmospheric circulation manifested as a too strong SPCZ clearly cause biases of surface properties in the coupled simulation.

While errors in water properties and pathways are profound in the coupled simulation, and the source of the errors can be identified, it is more difficult to determine the impact of such biases on the model climate. Presumably tropical water mass biases

impact how ENSO is represented. Because the intermediate waters are potentially a large sink of anthropogenic carbon in both hemispheres, their representation will be an important component of predicting ocean uptake of carbon dioxide in future climate simulation, especially when models contain active ocean biogeochemistry. Finally, the profound influence on the structure of the subtropical gyre by the western boundary current and its separation latitude, not only on the structure of the thermocline and the NPIW, but also for the residence time of water masses in the subtropical gyre, needs to be recognized. It is important to note that the errors that we describe here are not alone to the CCSM3. In the case of the Kuroshio separation, thus far no parameterization has given satisfactory results for low resolution models, and even high resolution models do not completely accurately represent western boundary current when compared against satellite observations (Kelly et al, 2007). The impact of small scale mixing driven by tides near the Okhotsk Sea on NPIW generation indicates that even if the Kuroshio were well represented, problems would still remain. Studies such as this one point out the problem spots where focused modifications in the ocean component of the couple model could lead to substantial modifications. These modifications could include a representation of mixing in the passages in the Kuril Island Chain as well as better representation of dense water formation near Antarctica. These problems continue to challenge modelers as we work towards more realism in reproducing current climate and predicting future changes.

Acknowledgments.

This material is based upon work supported by the National Science Foundation under Grant Nos. 0451479 and 0726519. We also acknowlege the help of Young-Oh Kwon and Steve Yeager.

References

Doney, S.C., and M.W. Hecht, 2001: Antarctic Bottom Water Formation and deep water chlorofluorocarbon distributions in a global ocean climate model: *J. Phys. Oceanogr.*, **32,** 1642-1666.

Collins, W. D., C. M. Bitz, M. L. Blackmon, G. B. Bonan, C. S. Bretherton, J. A. Carton, P, Chang, S, C. Doney, J, J. Hack, T. B. Henderson, J. T. Kiehla, W. G. Large, D. S. McKenna, B. D. Santerf, and R. D. Smith, 2006a: The Community Climate System Model Version 3 (CCSM3). *J. Climate*, **19**, 2122-2143.

Collins, W. D., P. J. Rasch, B. A. Boville, J. J. Hack, J. R. McCaa, D. L. Williamson, B. P. Briegleb, C. M. Bitz, S. Lin, and M. Zhang, 2006b: The Formulation and Atmospheric Simulation of the Community Atmosphere Model Version 3 (CAM3). *J. Climate*, **19**, 2144-2161.

Conkright, M.E., R. A. Locarnini, H.E. Garcia, T.D. O'Brien, T.P. Boyer, C. Stephens, J.I. Antonov, 2002: *World Ocean Atlas 2001: Objective Analyses, Data Statistics, and Figures, CD-ROM Documentation.* National Oceanographic Data Center, Silver Spring, MD, 17 pp.

daSilva, A., A. C.Young, and S. Levitus, 1994: *Atlas of surface marine data 1994, volume 1: Algorithms and procedures. Tech. Rep. 6.* U.S.Department of Commerce, NOAA, NESDIS.

England M. H., 1992: On the formation of Antarctic Intermediate and Bottom Water in ocean general circulation models. *J. Phys. Oceanogr.*, **22**, 918–926.

Gent, P. R, F. O. Byrn, G. Danabasoglu, K. Lindsay, D. Tsumune, M. W. Hecht, and S. C. Doney, 2006: Ocean Chlorofluorocarbon and Heat Uptake during the Twentieth Century in the CCSM3. *J. Climate*, **19**, 2366-2381.

——, and G. Danabasoglu, 2004: Heat uptake and the thermohaline circulation in the Community Climate System Model, version 2. *J. Climate*, **17,** 4058–4069.

——, and J. C. McWilliams, 1990: Isopycnal mixing in ocean circulation models. *J. Phys. Oceanogr.,* **20,** 150–155.

Emile-Geay, J., M. A. Cane, N. Naik, R. Seager, A. C. Clement, and A. van Geen, 2003: Warren revisited: Atmospheric freshwater fluxes and ‘‘Why is no deep water formed in the North Pacific’’. *J. Geophys. Res.*, **108**, 3178, doi:10.1029/2001JC001058.

Hautala, S.L., D.H. Roemmich and W.J. Schmitz, Jr., 1994: Is the North Pacific in Sverdrup balance along 24N? *J. Geophys. Res.*, **99**: 16,041-16,052

Hautala, S.L. and D. H. Roemmich, 1998: Subtropical mode water in the Northeast Pacific Basin. *J. Geophys. Res*., **103**, 13,055-13,066.

Kelly, K.A., L. Thompson, W. Cheng, and E.J. Metzger, 2007: Evaluation of HYCOM in the Kuroshio Extension region using new metrics, J. Geophys. Res., **112**, 10.1029/2006JC003614, 2007.

Kobayashi, T., 1999: Study of the formation of North Pacific Intermediate Water by a general circulation model and the particle-tracking method 1. A pitfall of general circulation model studies. *J. Geophys. Res.*, **104**, 5423-5440, 10.1029/1998JC900084.

Kobayashi, T., 2000: Study of the formation of North Pacific Intermediate Water by a general circulation model and the particle-tracking method: 2. Formation mechanism of salinity minimum from the view of the "critical gradient" of the Oyashio mixing ratio. *J. Geophys. Res.,* **105**, 1055-1070, 10.1029/1999JC900261.

Ladd, C. and L. Thompson, 2000: Formation Mechanisms for North Pacific Central and Eastern Subtropical Mode Waters. *J. Phys. Oceanogr.*, **30**, 868-887.

Ladd, C. and L. Thompson, 2001: Water Mass Formation in an Isopycnal Model of the North Pacific. *J. Phys. Oceanogr*., *31*, 1517-1537.

Large, W. G., and G. Danabasoglu, 2006: Attribution and Impacts of Upper-Ocean Biases in CCSM3. *J. Climate,* **19**, 2325-2346

Large, W.G., J.C. McWilliams, and S.C. Doney, 1994: Oceanic vertical mixing: A review and a model with a vertical K-profile boundary layer parameterization. **32**, *Rev Geophys.*, 363-403.

Mecking, S., M. J. Warner, C. E. Greene, S. L. Hautala, and R. E. Sonnerup, 2004: Influence of mixing on CFC uptake and CFC ages in the North Pacific thermocline. *J. Geophys. Res.*, **109,** C07014, doi:10.1029/2003JC001988.

Montenegro, A, M. Eby, A. J. Weaver, and S. R. Jayne, 2007: Response of a climate model to tidal mixing parameterization under present day and last glacial maximum conditions. *Ocean Model*., **19**, 125-137.

Nakamura, T., T. Toyoda, Y. Ishikawa, and T. Awaji, 2006: Effects of tidal mixing at the Kuril Straits on North Pacific ventilation: Adjustment of the intermediate layer revealed from numerical experiments, J. Geophys. Res., **111**, C04003, doi:10.1029/2005JC003142.

Qiu, B, and R. X Huang, 1995: Ventilation of the North Atlantic and North Pacific : Suduction and Subduction. *J. Phys. Oceanogr*., **25**, 2374-2390.

Rhines, P. B., andW. R. Young, 1982: A theory of the wind-driven circulation.

Part I: Mid-ocean gyres. *J. Mar. Res.*, **40** (Suppl), 559–596.

Suga, T; Motoki, K; Aoki, Y; Macdonald, AM. 2004: The North Pacific climatology of winter mixed layer and mode waters. *J. Phys. Oceanogr.*, **34**, 3-22.

Talley, L. D. 1993: Distribution and formation of North Pacific intermediate water. *J. Phys. Oceanogr*., **23**, 517-537.

Talley, L. D., 1997: North Pacific Intermediate Water Transports in the Mixed Water Region. *J. Phys. Oceanogr.*, **27**, 1795–1803.

Ueno, M., and I. Yasuda, 2000: Distribution and formation of the mesothermal structures (temperature inversions) in the North Pacific Subarctic Regions. J. Geophys. Res., **105** (C7), 16885-16898.

Vallis, G. K., 2006: *Atmospheric and Oceanic Fluid Dynamics*. Cambridge Univ. Press, 745 pp.

Weesel, S. R., and F. O. Bryan, 2006: Climate impacts of systematic errors in the simulation of the path of the North Atlantic Current. *Geophys. Res. Let.*, **33**, L19708, doi:10.1029/2006GL027669.

Yamanaka, G., Y. Kitamura, and M. Endoh, 1998: Formation of North Pacific Intermediate Water in Meteorological Research Institute ocean general circulation model.

1. Subgrid-scale mixing and marginal sea fresh water. *J. Geophys. Res*., **103**, 30885-30903.

Yasuda, I., K. Okuda, and Y. Shimizu, 1996: Distribution and Modification of North Pacific Intermediate Water in the Kuroshio-Oyashio Interfrontal Zone. J. Phys. Oceanogr., **26**, 448–465.

.

List of Figures

FIG. 1. Vertical cross sections of annual mean salinity (units: psu) averaged between 160° E and 180° E from WOA (a), CPL (b), and OCN (c), respectively. The white lines in all panels mark the 25.6 and 26.8 kg m^{-3} σ_θ surfaces.

FIG. 2. Annual mean salinity distribution (units: psu) on σ_θ =25.6 kg $m^{-3}$from WOA (a), CPL (c) and OCN (e), and σ_θ =26.8 kg m^{-3} WOA (b), CPL (d), and OCN (f). White lines mark the local winter (March in the Northern Hemisphere and September in the Southern Hemisphere) outcropping of the isopycnal.

FIG. 3. Barotropic stream function as predicted from Sverdrup theory using wind forcing from (a) CPL and (b) OCN models while (c) shows the barotropic stream function from CPL. For a direct comparison (d) shows the barotropic stream function as a function of longitude at 30N from CPL (dashed-dotted), and OCN (dashed) as well as the prediction from Sverdrup theory for CPL forcing (dotted), and OCN forcing (solid). Units are Sverdrups 10^6 m^3s^{-1}.

FIG. 4. Meridional overturning circulation in the Pacific Ocean in the top 1100 m shown for (a) CPL and (b) OCN. Units are Sverdrups 10^6 m^3s^{-1}.

FIG. 5. Differences between model and WOA annual mean SSS and SST. Shown is (a) CPL-WOA SST (b) CPL-WOA SSS, (c) OCN-WOA SST, and (d) OCN-WOA SSS. SST differences are in units of °C and SSS differences are in units of psu.

FIG. 6. Annual mean buoyancy forcing from freshwater and heat fluxes averaged between 120° E and 110° W. Shown in (a) is (a) CPL-OCN evaporation (dashed), precipitation (dashed-dotted) and total fresh water flux (solid) in mm day^{-1}. (b) shows the fresh water forcing for OCN with evaporation-precipitation (dotted-dashed) and relaxation (solid) in mm/day. (c) Shows CPL-OCN for each component of the heat flux (Wm^{-2}) with turbulent heat flux (dotted), long-wave radiation (dashed), short wave radiation(dashed-dotted) and total heat flux (solid) and (d) shows zonally averaged SST.

FIG. 7. March mixed layer depth (MLD) from (a) WOA (top panel), (b) CPL and (c) OCN. MLD is based on the potential density criterion, namely, a density change of 0.125 (σ_θ) from the ocean surface. Three boxes in the western subarctic gyre, the western subtropical gyre and the eastern subtropical gyre are marked as A, 164° C to 172° C and 52° N to 57° N, B, 145° E to 160° E and 30° N to 40° N, and C, 148° N and 135° W, and 25° N and 35° N, respectively.

FIG. 8. Shown is the MLD (m) as a function of time for one year beginning in September. The columns are the area averaged MLD for the three regions identified in Figure 7. The first row (a, b and c) is the MLD from the observations (solid line), and the full model runs OCN (dotted line) and CPL (dashed line). The next row (d, e and f) are results from the one-dimensional KPP model with Levitus initial conditions, (g,h, and I) use OCN initial conditions, and (j,k and l) use CPL initial conditions. For the bottom three rows, the forcing used for the one-dimensional model is observed (solid), OCN (dotted) and CPL (dashed).

FIG. 9. Annual mean potential temperature-salinity diagram at the intersections at 180 °E and (a) 40 °N, (b) 20 °N, (c) equator, (d) 20 °S, (e) 40 °C S, respectively. Data from OCN (dotted), CPL (solid) and WOA (dashed) is shown.

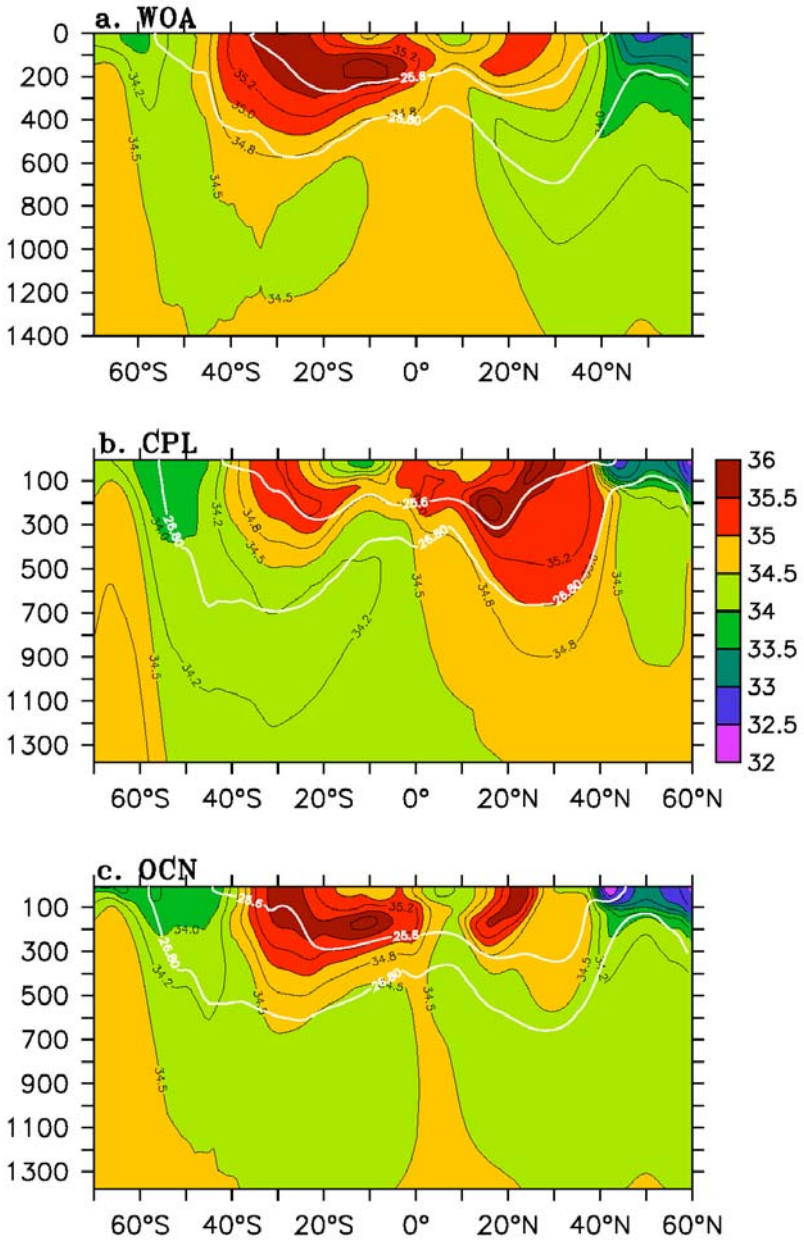

FIG. 1. Vertical cross sections of annual mean salinity (units: psu) averaged between 160° E and 180° E from WOA (a), CPL (b), and OCN (c), respectively. The white lines in all panels mark the 25.6 and 26.8 kg m^{-3} σ_θ surfaces.

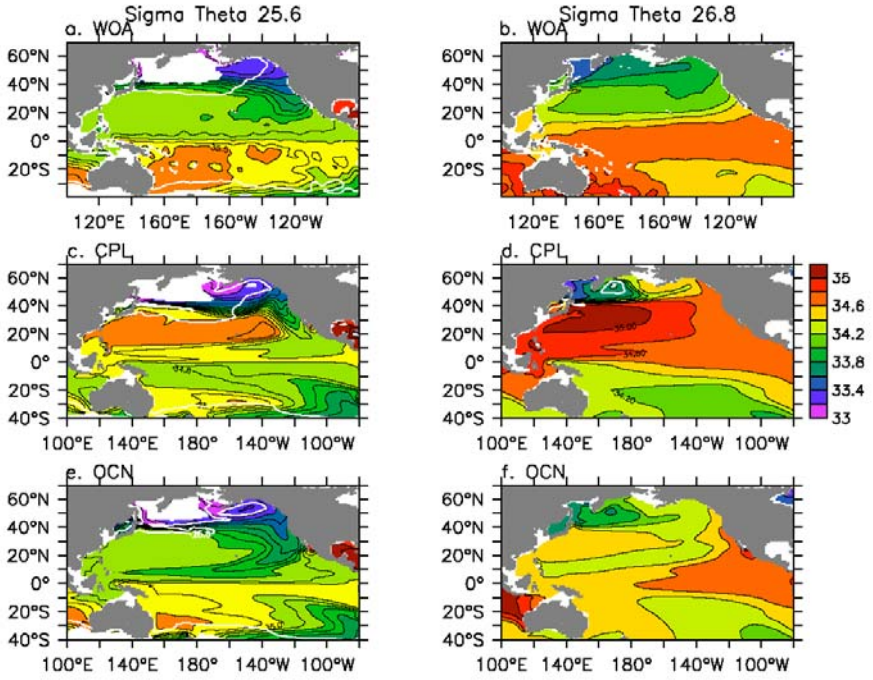

FIG. 2. Annual mean salinity distribution (units: psu) on σ_θ =25.6 kg m^{-3}from WOA (a), CPL (c) and OCN (e), and σ_θ =26.8 kg m^{-3} WOA (b), CPL (d), and OCN (f). White lines mark the local winter (March in the Northern Hemisphere and September in the Southern Hemisphere) outcropping of the isopycnal.

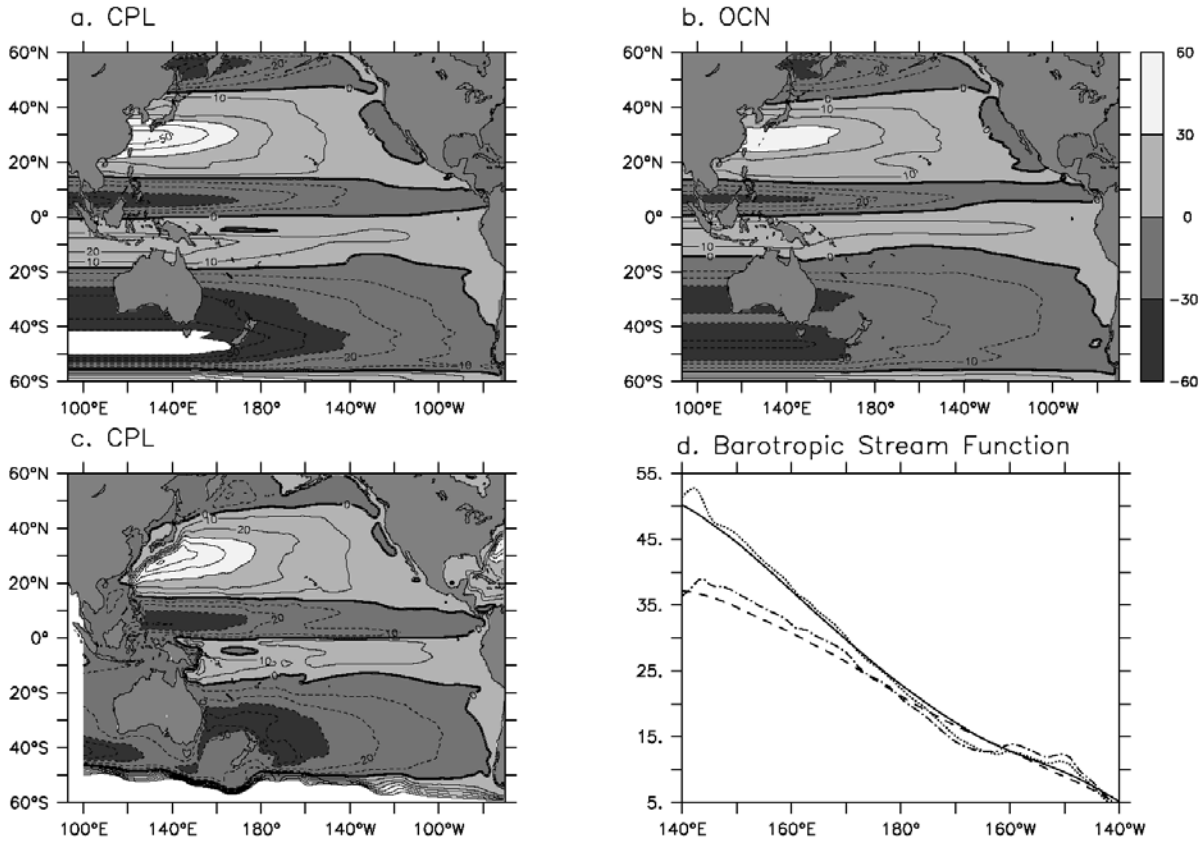

FIG. 3. Barotropic stream function as predicted from Sverdrup theory using wind forcing from (a) CPL and (b) OCN models while (c) shows the barotropic stream function from the CPL model run (note the circulation closes in the western boundary). (d) shows the barotropic stream function as a function of longitude at 30N from CPL (dotted), and

OCN (dash-dotted) as well as the prediction from Sverdrup theory for CPL forcing (solid), and OCN forcing (dashed). Units are Sverdrups [10^6 m^3s^{-1}].

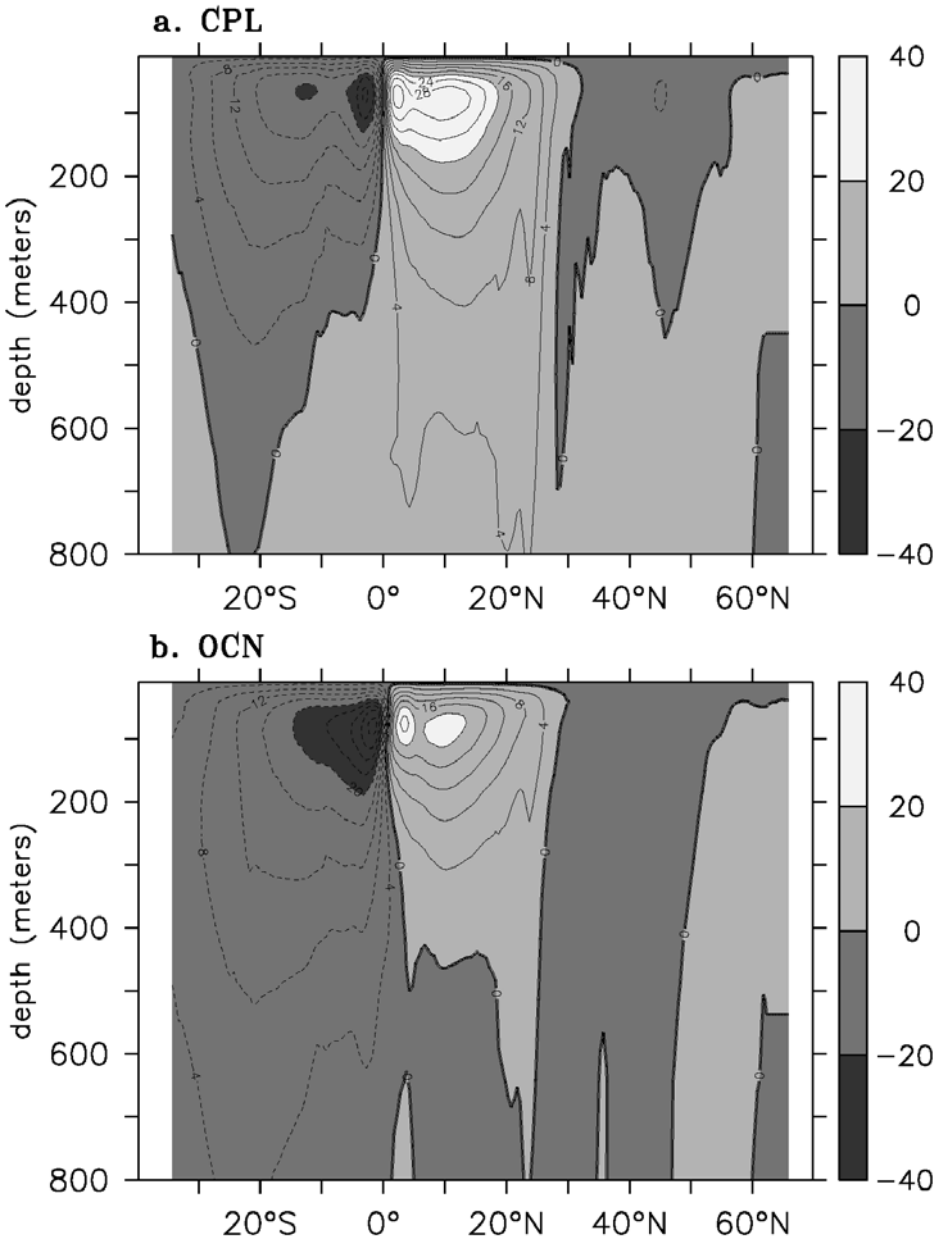

FIG. 4. Meridional Eulerian overturning circulation in the Pacific Ocean in the top 1100 m shown for (a) CPL and (b) OCN. Units are Sverdrups [10^6 m^3s^{-1}.]

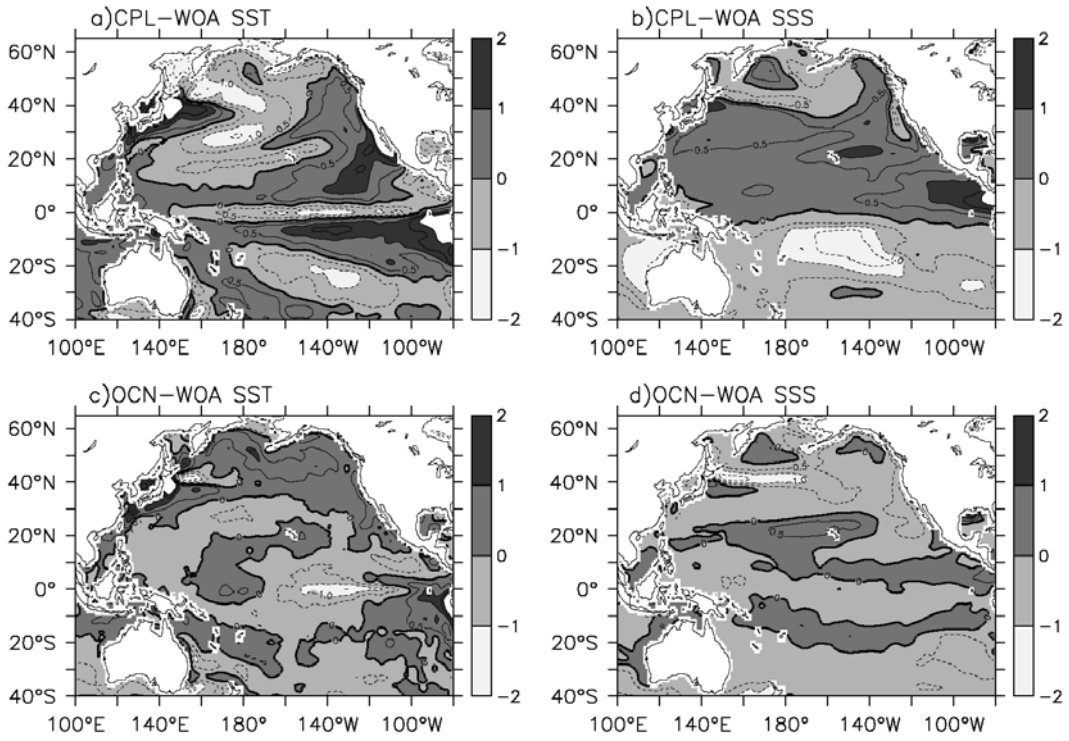

FIG. 5. Differences between model and WOA annual mean SSS and SST. Shown is (a) CPL-WOA SST (b) CPL-WOA SSS, (c) OCN-WOA SST, and (d) OCN-WOA SSS. SST differences are in units of $^{\circ}$C and SSS differences are in units of psu.

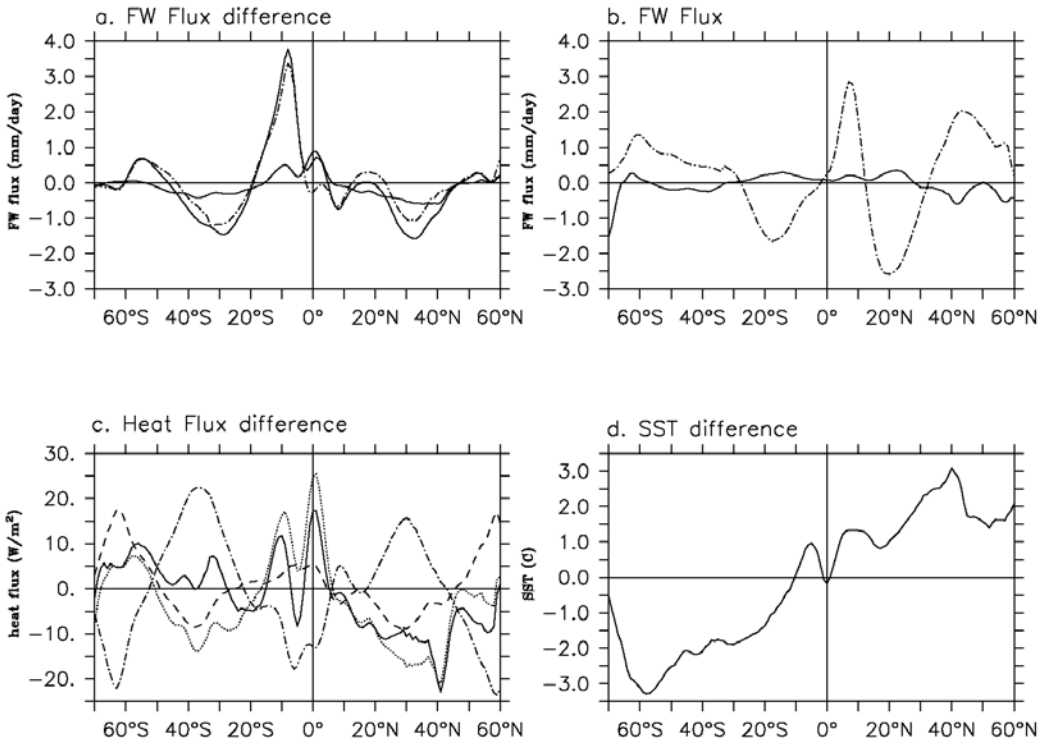

FIG. 6. Annual mean buoyancy forcing from freshwater and heat fluxes averaged between 120°E and 110°W. Shown in (a) is CPL-OCN evaporation (dashed), precipitation (dashed-dotted) and total fresh water flux (solid) in mm day^{-1}. (b) shows the fresh water forcing for OCN with evaporation-precipitation (dotted-dashed) and relaxation (solid) in mm/day. (c) Shows CPL-OCN for each component of the heat flux (Wm^{-2}) with turbulent heat flux (dotted), long-wave radiation (dashed), short wave radiation(dashed-dotted) and total heat flux (solid) and (d) shows zonally averaged SST.

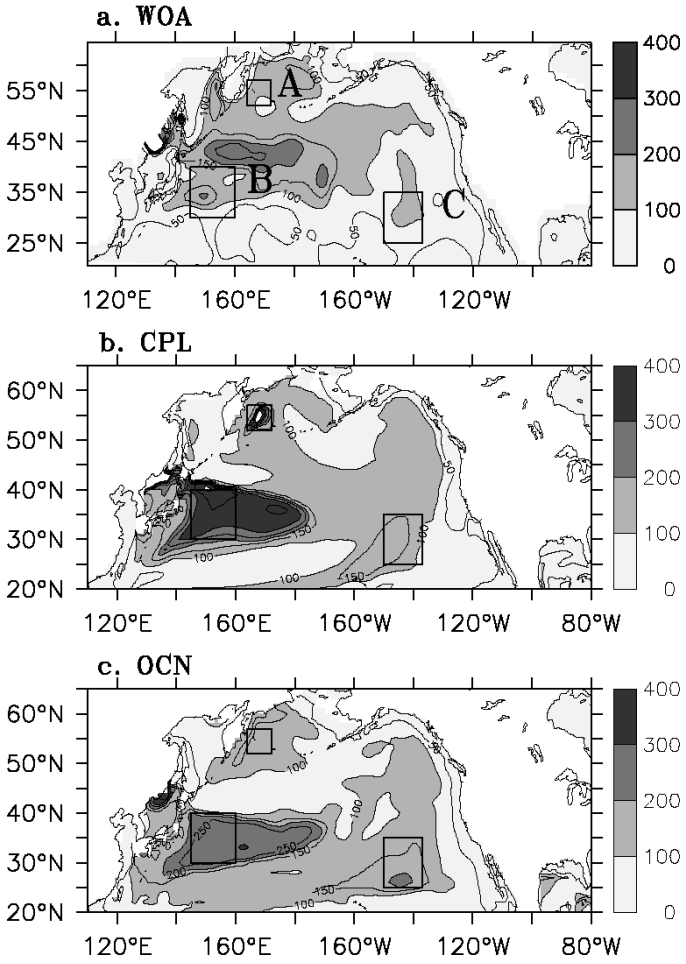

FIG. 7. March mixed layer depth (MLD) from (a) WOA (top panel), (b) CPL and (c) OCN. MLD is based on the potential density criterion, namely, a density change of 0.125 (σ_θ) from the ocean surface. Three boxes in the western subarctic gyre, the western subtropical gyre and the eastern subtropical gyre are marked as A, 164° C to 172° C and 52° N to 57° N, B, 145° E to 160° E and 30° N to 40° N, and C, 148° N and 135° W, and 25° N and 35° N, respectively.

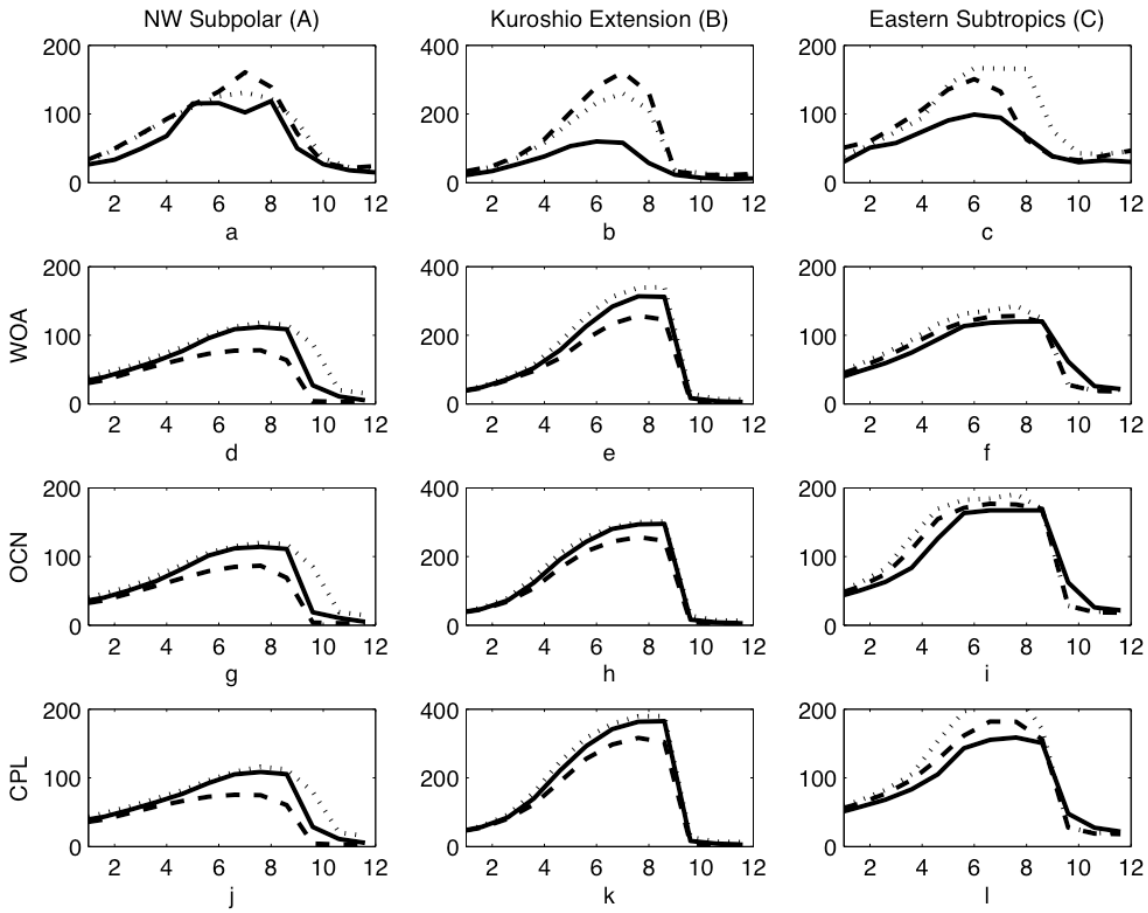

FIG. 8. Shown is the MLD (m) as a function of time for one year beginning in September. The columns are the area averaged MLD for the three regions identified in Figure 7. The first row (a, b and c) is the MLD from the observations (solid line), and the full model runs OCN (dotted line) and CPL (dashed line). The next row (d, e and f) are results from the one-dimensional KPP model with Levitus initial conditions, (g,h, and i) use OCN initial conditions, and (j,k and l) use CPL initial conditions. For the bottom three rows, the forcing used for the one-dimensional model is observed (solid), OCN (dotted) and CPL (dashed).

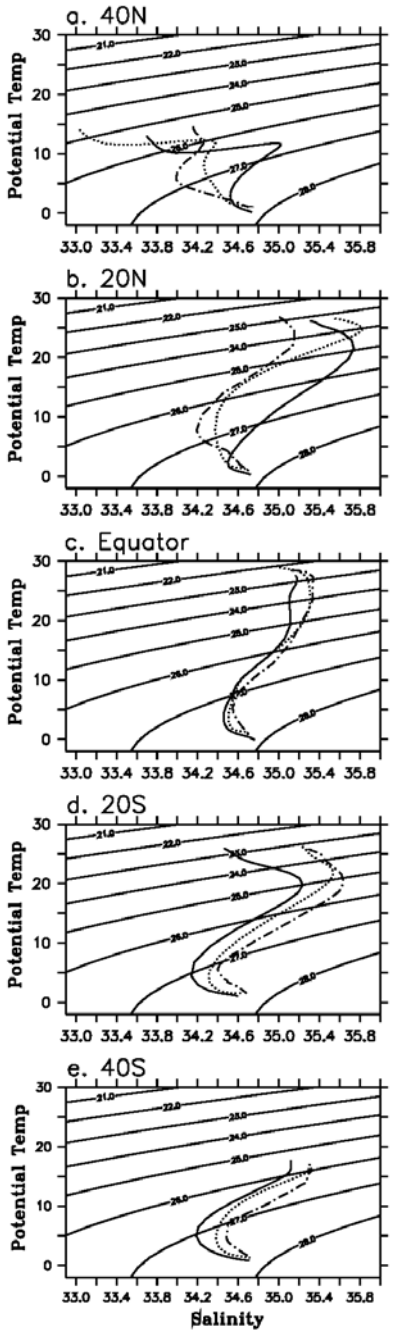

FIG. 9. Annual mean potential temperature-salinity diagram at the intersections at 180 ° E and (a) 40 ° N, (b) 20 ° N, (c) equator, (d) 20 ° S, (e) 40 ° C S, respectively. Data from OCN (dotted), CPL (solid) and WOA (dashed) is shown.